# 3D Prostate TRUS Segmentation Using Globally Optimized Volume-Preserving Prior

Wu Qiu[1], Martin Rajchl[1], Fumin Guo[1], Yue Sun[1], Eranga Ukwatta[2], Aaron Fenster[1], and Jing Yuan[1]

[1] Robarts Research Institute, University of Western Ontario, London, ON, Canada
[2] Department of Biomedical Engineering, Johns Hopkins University, Baltimore, MD, United States

**Abstract.** An efficient and accurate segmentation of 3D transrectal ultrasound (TRUS) images plays an important role in the planning and treatment of the practical 3D TRUS guided prostate biopsy. However, a meaningful segmentation of 3D TRUS images tends to suffer from US speckles, shadowing and missing edges etc, which make it a challenging task to delineate the correct prostate boundaries. In this paper, we propose a novel convex optimization based approach to extracting the prostate surface from the given 3D TRUS image, while preserving a new global volume-size prior. We, especially, study the proposed combinatorial optimization problem by convex relaxation and introduce its dual continuous max-flow formulation with the new bounded flow conservation constraint, which results in an efficient numerical solver implemented on GPUs. Experimental results using 12 patient 3D TRUS images show that the proposed approach while preserving the volume-size prior yielded a mean DSC of $89.5\% \pm 2.4\%$, a MAD of $1.4 \pm 0.6$ $mm$, a MAXD of $5.2 \pm 3.2$ $mm$, and a VD of $7.5\% \pm 6.2\%$ in $\sim$ 1 minute, deomonstrating the advantages of both accuracy and efficiency. In addition, the low standard deviation of the segmentation accuracy shows a good reliability of the proposed approach.

**Keywords:** Image Segmentation, 3D Prostate TRUS Image, Convex Optimization, Volume Preserving Constraint.

## 1 Introduction

Prostate adenocarcinoma (PCa) is the most common non-cutaneous malignancy in American men with over $200,000$ new cases diagnosed each year [1]. Definitive diagnosis of PCa requires a transrectal ultrasound (TRUS) guided biopsy [2]. Recent developments of biopsy systems using the fusion of 3D prostate TRUS and MR imagesdemonstrated an increased positive yield and greater number of cores with higher Gleason grade [3]. An accurate and efficient automated or semi-automated 3D prostate TRUS segmentation is highly beneficial for the registration of the 3D MR prostate image to TRUS in those systems [4,5,6]. However, the accurate segmentation of 3D TRUS images often suffers from the low quality of TRUS images, as shown in Fig. 1(a), such as US speckles, shadowing

P. Golland et al. (Eds.): MICCAI 2014, Part I, LNCS 8673, pp. 796–803, 2014.

due to calcifications, missing edges or texture similarities between the inner and outer regions of the prostate etc [7], which make it challenging to implement such an automated or semi-automated 3D TRUS segmentation method. The target of this study is to develop an accurate, efficient and reliable 3D prostate TRUS image segmentation approach.

Even though there are extensive studies [8] in delineating prostate boundaries from 3D TRUS images, most of them rely on classifiers, atlas or deformable models. The deformable model based methods typically used a 3D deformable surface as initialization, which is then automatically refined by forces, such as image gradient and smoothness of the surface [9,10,11]. These methods were designed and implemented in a local optimization style, such that the discrete propagation step-size is restricted to be small enough to achieve convergence and it results in low computational inefficiency. In addition, the local optimization based segmentation methods are sensitive to the initialization, and would leak at the locations with weak edges. The direct 3D segmentation methods worked well for the reported applications, but are time consuming and require intensive user interactions that leads to a high observer variability. Classifier based technique, such as support vector machine (SVM), depended on the training datasets [12]; however, the image quality in the datasets significantly varied due to different US machine settings, which prevents this technique from practical clinical applications.

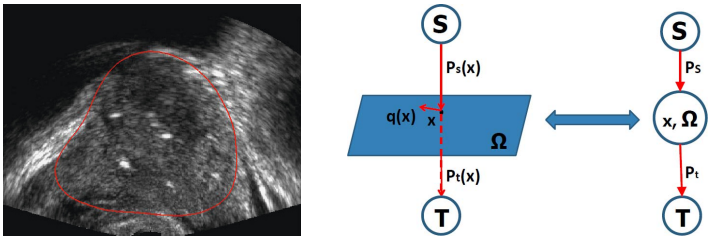


(a) (b)

**Fig. 1.** Fig. 1(a) illustrates the typical 2D view of a 3D TRUS image with US speckles, calcifications, weak edge information etc. Fig. 1(b) shows the flow configurations of the proposed continuous max-flow model.

**Contributions:** In this study, we propose a novel convex optimization based approach to segmenting the prostate from the given 3D TRUS image while enforcing the new global volume-size prior, which is inspired by the work [13]. Such volume-size prior provides a global geometric description for the interesting object region and helps the segmentation procedure avoid suffering from low image quality of TRUS images. We, especially, introduced a non-smooth $L1$ volume prior function (its derivative cannot be directly computed) and employed a continuous convex optimization framework, which yields better efficiency and accuracy while avoiding metrification errors, and results in an efficient numerical

solver implemented on GPUs. Promising experimental results demonstrate the advantages of the proposed approach in both accuracy and efficiency, along with a great reliability.

## 2 Methods

In this section, we introduce a novel global/convex optimization based approach to segmenting an input 3D prostate TRUS image $I(x)$ into the prostate region $\mathcal{R}_P$ and the background region $\mathcal{R}_B$, while imposing a new volume-size prior of the prostate region. Actually, the volume-size information about the interesting object region provides a global geometric description for the image segmentation task; on the other hand, such knowledge can be easily obtained in most applications by learning the given training images or the other information sources. In this work, the prostate volume-size $\mathcal{V}$ of the specified patient is calculated from the pre-segmented 3D prostate T2-weighted MR image of the same patient (see Sec. 3 for more details of the pipeline and initializations). Note: the exact volume-size is not necessary for the proposed approach in this paper and the approximation of the prostate volume could also be obtained from the other image source, for example the 3D prostate CT image.

Especially, we propose a new continuous min-cut formulation with the introduced volume-size preserving prior and solve the challenging combinatorial optimization problem by means of convex relaxation. To this end, a novel continuous max-flow model with a bounded unvanished flow conservation condition, which is in contrast to the classical max-flow models with the exact vanishing flow conservation constraint [14,15,16]; moreover, we show its duality to the convex relaxaion of the studied continuous min-cut formulation with the volume-size preserving constraint, which directly derives an efficient duality-based numerical scheme implementing on the modern parallel computing platforms, e.g. GPUs.

**Continuouse Min-Cut Model with Volume-Size Preserving.** In this work, the intensity appearance information of the input TRUS image $I(x)$, i.e. the corresponding intensity probability density functions (PDFs) of both the prostate region $\mathcal{R}_P$ and background region $R_B$, is utilized to assist the prostate TRUS image segmentation task. Such intensity appearance models provide a global descriptor of both regions of prostate and background in image statistics, which can be learned by either sampled pixels or the specified training datasets. Let $\omega^P(I(x))$ be the intensity PDF of the prostate region $\mathcal{R}_P$ appearing on the input image $I(x)$, which actually encodes the probability of each pixel $x$ belonging to the region $\mathcal{R}_P$; and $\omega^B(I(x))$ the PDF of the background region $\mathcal{R}_B$. In consequence, we define the cost function $D_t(x)$ of labeling each pixel $x$ to be in the prostate region $\mathcal{R}_P$, and $D_s(x)$ the labeling cost function w.r.t. the background region $\mathcal{R}_B$, by the log-likelihoods of the respective PDFs, i.e.

$$D_t(x) \,=\, -\log\left(\omega^P(I(x))\right), \quad D_s(x) \,=\, -\log\left(\omega^B(I(x))\right).$$

Let $u(x) \in \{0,1\}$ be the indicator/labeling function of the prostate region $\mathcal{R}_P$, where $u(x) = 1$ denotes the pixel $x$ inside $\mathcal{R}_P$, and otherwise outside $\mathcal{R}_P$.

With this regard, the classical way to segment the input TRUS image of $I(x)$ is to minimize the min-cut energy function [14,15], e.g. the spatially continuous min-cut model [15]:

$$\min_{u(x)\in\{0,1\}} E(u) := \langle u, D_t\rangle + \langle 1-u, D_s\rangle + \int_\Omega g(x)\,|\nabla u|\,dx \tag{1}$$

where $g(x) \geq 0$ stands for the weight function assocaited with image edges, hence the weighted total-variation function measures the weighted area of the prostate region. In this paper, we also enforce preserving the specified volume-size $\mathcal{V}$ in the continuous min-cut model (1) by penalizing the difference between the volume of the prostate region $\mathcal{R}_P$ and $\mathcal{V}$, such that

$$\min_{u(x)\in\{0,1\}} E(u) \,+\, \gamma\,|\mathcal{V} - \int_\Omega u\,dx|\,, \tag{2}$$

where $\gamma > 0$ is a positive parameter to impose a soft volume-size constraint, which is set once for segmenting the whole dataset.

In this work, we solve the introduced challenging combinatorial optimization problem (2) by its convex relaxation, i.e.

$$\min_{u(x)\in[0,1]} E(u) \,+\, \gamma\,|\mathcal{V} - \int_\Omega u\,dx| \tag{3}$$

where the binary labeling constraint $u(x) \in \{0,1\}$ in (2) is relaxed to the convex set of $u(x) \in [0,1]$. Given the convex energy function of (3), it results in the convex optimization problem which is much simpler than its original combinatorial optimization model (2) in mathematics.

**Continuous Max-Flow Formulation with Bounded Flow Conservation.** Now we propose a new *continuous max-flow model* along with the same flow configuration as in [15] (also see Fig. 1(b) for illustration), such that:

$$\max_{p_s,p_t,q,r} \int_\Omega p_s\,dx \,+\, r\mathcal{V} \tag{4}$$

subject to

– *Flow capacity constraints*: the source, sink and spatial flows $p_s(x)$, $p_t(x)$ and $q(x)$ suffice:

$$p_s(x) \,\leq\, D_s(x)\,, \quad p_t(x) \,\leq\, D_t(x)\,, \quad |q(x)| \,\leq\, g(x)\,; \quad \forall\, x \,\in\, \Omega\,; \tag{5}$$

– *Bounded flow conservation constraints*: the total flow residue is not vanishing at any pixel $x \in \Omega$ but bounded, *i.e.*

$$\big(\operatorname{div} q \,-\, p_s \,+\, p_t\big)(x) \,=\, r \,\in\, [-\gamma,\gamma]\,, \quad \forall\, x \,\in\, \Omega\,. \tag{6}$$

Obviously, the proposed continuous max-flow model (4) is distinct from the classical continuous max-flow formulation investigated in [15], in that the flow

residue at each pixel $x$ for (4) does not vanish, but is equal to a constant value $r$ which is bounded within the range $[-\gamma, \gamma]$, while a strict flow conservation condition is required for the classical max-flow model of [15]. In addition, the total energy of (4) is evaluated by the total flow streaming from the source plus the total flow residue $r\mathcal{V}$.

Follow the same analysis proposed in [15,16], we can prove

**Proposition 1.** *The* continuous max-flow model (4) *and the convex relaxation of* volume-preserving continuous min-cut model (3) *are dual (equivalent) to each other, i.e.*

$$(4) \iff (3)\,.$$

The proof is omitted due to the limited space.

Clearly, maximizing the proposed *continuous max-flow model* (4) enjoys great numerical advantages such that it successfully avoids directly tackling the non-linear and non-smooth function terms of the studied *convex relaxed optimization problem* (3). Additionally, it also derives an efficient multiplier-augmented algorithm based on the modern convex optimization theory (see [15] for details), which can be readily implemented on the modern parallel computing platforms, i.e. GPUs, to significantly improve the computational efficiency in practice.

## 3 Experiments and Results

**Image Acquisition:** All subjects involved in this study were suspected to have tumors identified by multi-spectral MR imaging. The images were acquired with a rotational scanning 3D TRUS-guided prostate biopsy system, which made use of a commercially available end-firing TRUS transducer (Philips, Bothell WA). The size of each 3D image was $448 \times 448 \times 350$ voxels of size $0.19 \times 0.19 \times 0.19 mm^3$. 12 patient images were tested in this paper.

**Implementations:** The prostate volume size of each patient used as the volume preserving prior was calculated from the manually pre-segmented prostate T2 weighted MR image of the same patient by three experts. The proposed approach was initialized by a closed surface, which is constructed by the thin-plate spline with positioning ten initial points on the boundary of the prostate (six

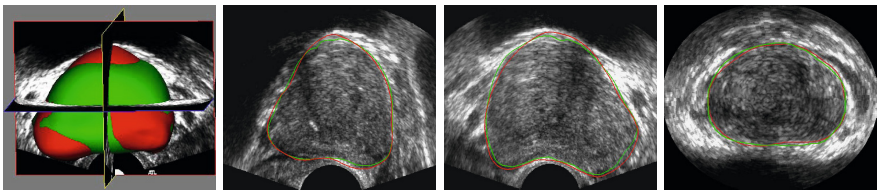

**Fig. 2.** Segmented ventricles (green contour, DSC: 92.5%) overlapped with manual segmentations (red contour). Left to right: segmented surface, sagittal view, coronal view, and transverse view.

at the transverse view, four at the sagittal view) [17,18]. The inside and outside voxels of the estimated surface are used to generate prior intensity probability density functions (PDFs) for the prostate and background regions, and the cost functions $D_{s,t}(x)$ were calculated by the log-likelihood of the respective intensity PDFs [18]. The closed surface also defines the initial guess of the prostate region and gives the starting value of the labeling function $u(x)$ for the proposed approach. The proposed algorithm was implemented on the parallel computing architecture (CUDA, NVIDIA Corp., Santa Clara, CA) and the user interface in Matlab (Natick, MA). The GPU based algorithm was developed and integrated with the non-optimized Matlab program, which ran on a Windows desktop with an 4-core Intel i7-2600 CPU (3.4 GHz) and a NVIDIA Geforce 5800X GPU.

**Evaluation Metrics:** A manual segmentation of each image used as the ground truth was compared to the algorithm segmented result, using *volume-based metrics*: Dice similarity coefficient (DSC); *distance-based metrics*: the mean absolute surface distance (MAD) and maximum absolute surface distance (MAXD); and *volume measurement metrics*: absolute volume difference (VD), $|(V_{Manual} - V_{algorithm})/V_{Manual}|$.

**Table 1.** Segmentation results of 12 patient 3D TRUS images in terms of DSC, MAD, MAXD, and VD, represented as Mean ± SD, using the continuous max-flow algorithm with ($CMF_{VP}$) and without ($CMF$ [15]) volume preserving constraint

| | DSC (%) | MAD (mm) | MAXD (mm) | VD (%) |
|---|---|---|---|---|
| $CMF_{VP}$ | $89.5 \pm 2.4$ | $1.4 \pm 0.6$ | $5.2 \pm 3.2$ | $7.5 \pm 6.2$ |
| $CMF$ | $78.3 \pm 7.4$ | $3.5 \pm 1.3$ | $9.4 \pm 3.0$ | $15.0 \pm 10.2$ |

**Accuracy:** Figure 2 shows one algorithm segmented prostate (green contours) and manual delineations (red contours) of one patient, visually demonstrating a good agreement. Table 1 shows the mean quantitative segmentation results for 12 patient images using the proposed method. Our approach obtained a mean DSC of $89.5\% \pm 2.4\%$, a MAD of $1.4 \pm 0.6$ $mm$, a MAXD of $5.2 \pm 3.2$ $mm$, and a VD of $7.5\% \pm 6.2\%$ for the used 12 patient images. More specifically, the proposed continous max-flow algorithm with the volume-preserving prior impoved the accuracy by more than 11% in terms of DSC comparing to the continous max-flow algorithm without priors [15].

**Computational Efficiency:** The mean segmentation time of the GPU implemented algorithm for one 3D TRUS image, calculated as a mean time using all 3D TRUS images, was $35 \pm 5$ s in addition to $30 \pm 5$ s for initialization, hence less than 1.2 minutes for a given 3D TRUS image in avarage.

## 4 Discussion and Conclusion

This paper proposes an accurate and efficient segmentation algorithm for 3D prostate TRUS images. The experimental results using 12 patient images show

that the proposed method yielded a mean DSC of $89.5\% \pm 2.4\%$, a MAD of $1.4 \pm 0.6$ $mm$, a MAXD of $5.2 \pm 3.2$ $mm$, and a VD of $7.5\% \pm 6.2\%$ within 1.2 minutes compared to manual segmentations. The low standard deviation of the segmentation accuracy in terms of metrics above shows a good consistency during all the segmentations, which is an important aspect in clinic. We compared our proposed approach with the prostate segmentation algorithms using 3D TRUS images, which used similar evaluation metrics and provided best segmentation accuracy in a literature reviewing paper [8]. The mean DSC of 89.5% obtained by our method are comparable to a volume overlap of 83.5% obtained by Tutar *et al.* [9] and 86.4% obtained by Garnier *et al.* [11], and a volume overlap error of 6.63% obtained by Mahdavi *et al.* [10]. The mean MAD of 1.4 mm obtained by our method is comparable to 1.26 mm obtained by Tutar *et al.* [9]. In addition, the computational time of 35 seconds of our method excluding initialization time is less than 1-4 minutes obtained by Tutar *et al.* [9]. Although Mahdavi *et al.* [10] reported 14 seconds for one image segmentation in their experiments, their method required additional 1-3 minutes for modification. The method by Garnier *et al.* [11] required 26 seconds, but it was implemented in C language and the computation was limited in an user defined ROI. Note that the computation of the energy formulations $E(u)$ in (1) including the data cost functions $D_{s,t}(x)$ and the image edge weight function $g(x)$ were developed using a Matlab code and run on CPU, which could be parallelized or converted to the C program to speed up computation.

In conclusion, this paper proposed a novel globally optimized volume-preserving segmentation approach for 3D TRUS images. The quantitative validation results using different metrics (DSC, MAD, MAXD, and VD) showed that it is capable of delineating the prostate surface accurately and efficiently. Its performance results suggest that it may be suitable for the clinical use involving the image guided prostate biopsy procedures.

**Acknowledgments.** The authors are grateful for the funding support from the Ontario Research Fund (OFC) and the Canada Research Chairs (CRC) Program.

## References

1. Jemal, A., Siegel, R., Xu, J., Ward, E.: Cancer statistics, 2010. CA Cancer J. Clin. 60(5), 277–300 (2010)
2. Qiu, W., Yuchi, M., Ding, M., Tessier, D., Fenster, A.: Needle segmentation using 3D hough transform in 3D TRUS guided prostate transperineal therapy. Med. Phy. 40(4), 042902–1–13 (2013)
3. Leslie, S., Goh, A., Lewandowski, P.M., Huang, E.Y.H., de Castro Abreu, A.L., Berger, A.K., Ahmadi, H., Jayaratna, I., Shoji, S., Gill, I.S., Ukimura, O.: Contemporary image-guided targeted prostate biopsy better characterizes cancer volume, gleason grade and its 3d location compared to systematic biopsy. The Journal of Urology 187(suppl. 4), e827 (2050)

4. Sonn, G.A., Natarajan, S., Margolis, D.J., MacAiran, M., Lieu, P., Huang, J., Dorey, F.J., Marks, L.S.: Targeted biopsy in the detection of prostate cancer using an office based magnetic resonance ultrasound fusion device. The Journal of Urology 189(1), 86–92 (2013)
5. Qiu, W., Yuan, J., Ukwatta, E., Yue, S., Rajchl, M., Fenster, A.: Prostate segmentation: An efficient convex optimization approach with axial symmetry using 3d trus and mr images. IEEE Trans. Med. Imag. 33(4), 947–960 (2014)
6. Litjens, G., Toth, R., van de Ven, W., Hoeks, C., Kerkstra, S., van Ginneken, B., Vincent, G., Guillard, G., Birbeck, N., Zhang, J., et al.: Evaluation of prostate segmentation algorithms for mri: the promise12 challenge. Med. Imag. Anal. 18(2), 359–373 (2014)
7. Qiu, W., Yuan, J., Ukwatta, E., Tessier, D., Fenster, A.: 3D prostate segmentation using level set with shape constraint based on rotational slices for 3D end-firing TRUS guided biopsy. Med. Phy. 40(7), 072903–1–12 (2013)
8. Ghose, S., Oliver, A., Martí, R., Lladó, X., Vilanova, J., Freixenet, J., Mitra, J., Sidibé, D., Meriaudeau, F.: A survey of prostate segmentation methodologies in ultrasound, magnetic resonance and computed tomography images. Computer Methods and Programs in Biomedicine 108(1), 262–287 (2012)
9. Tutar, I.B., Pathak, S.D., Gong, L., Cho, P.S., Wallner, K., Kim, Y.: Semiautomatic 3D prostate segmentation from TRUS images using spherical harmonics. IEEE Trans. Med. Imaging 25(12), 1645–1654 (2006)
10. Mahdavi, S.S., Moradi, M., Wen, X., Morris, W.J., Salcudean, S.E.: Evaluation of visualization of the prostate gland in vibro-elastography images. Med. Imag. Anal. 15(4), 589–600 (2011)
11. Garnier, C., Bellanger, J.J., Wu, K., Shu, H., Costet, N., Mathieu, R., de Crevoisier, R., Coatrieux, J.L.: Prostate segmentation in HIFU therapy. IEEE Trans. Med. Imag. 30(3), 792–803 (2011)
12. Akbari, H., Fei, B.: 3D ultrasound image segmentation using wavelet support vector machines. Med. Phys. 39(6), 2972–2984 (2012)
13. Gorelick, L., Schmidt, F.R., Boykov, Y., Delong, A., Ward, A.: Segmentation with non-linear regional constraints via line-search cuts. In: Fitzgibbon, A., Lazebnik, S., Perona, P., Sato, Y., Schmid, C. (eds.) ECCV 2012, Part I. LNCS, vol. 7572, pp. 583–597. Springer, Heidelberg (2012)
14. Boykov, Y., Veksler, O., Zabih, R.: Fast approximate energy minimization via graph cuts. IEEE Trans. Patt. Anal. Mach. Intel. 23(11), 1222–1239 (2001)
15. Yuan, J., Bae, E., Tai, X.: A study on continuous max-flow and min-cut approaches. In: Davis, L., Malik, J. (eds.) IEEE CVPR, San Francisco, USA, pp. 2217–2224 (2010)
16. Yuan, J., Bae, E., Tai, X.-C., Boykov, Y.: A continuous max-flow approach to potts model. In: Daniilidis, K., Maragos, P., Paragios, N. (eds.) ECCV 2010, Part VI. LNCS, vol. 6316, pp. 379–392. Springer, Heidelberg (2010)
17. Yuan, J., Qiu, W., Ukwatta, E., Rajchl, M., Sun, Y., Fenster, A.: An efficient convex optimization approach to 3D prostate MRI segmentation with generic star shape prior. In: Ayache, N., Delingette, H., Golland, P., Mori, K. (eds.) Prostate MR Image Segmentation Challenge, MICCAI, vol. 7512. Springer (2012)
18. Qiu, W., Yuan, J., Ukwatta, E., Sun, Y., Rajchl, M., Fenster, A.: Dual optimization based prostate zonal segmentation in 3D MR images. Med. Imag. Anal. 18(4), 660–673 (2014)